Applied Physics B (2021) 127:144
https://doi.org/10.1007/s00340-021-07694-7

Applied Physics B
Lasers and Optics

Orientation of Co^{2+} dipoles in magnesium–aluminum spinel crystal

Yu Wang[1] · Weichong Wu[1] · Zhanda Zhu[1,2,3,4] · Yongling Hui[1,2,3,4] · Hong Lei[1,2,3,4] · Qiang Li[1,2,3,4]

Received: 22 July 2021 / Accepted: 20 September 2021 / Published online: 28 September 2021

Abstract
The nonlinear transmission curves of [100]- and [110]-cut Co^{2+}:$MgAl_2O_4$ crystals at 1.54 μm were measured experimentally. A phenomenological model was established to analyze the experimental results, in which resonant absorption in the Co^{2+}:$MgAl_2O_4$ crystal was characterized by four groups of linear dipoles oriented along the four body diagonals ([111], [1 11], [1 1 1] and [11 1] axis) of the unit cell. The theoretical calculations were in good agreement with the experimental measurement data. This work demonstrated that the transition dipoles were parallel to the four body diagonals of the Co^{2+}:$MgAl_2O_4$ unit cell. Meanwhile, absorption cross-sections of the ground state and excited state at 1.54 μm were calculated to be $\sigma_{gsa} = (3.6 \pm 0.3) \times 10^{-19}$ cm^2 and $\sigma_{esa} = (4.5 \pm 0.4) \times 10^{-20}$ cm^2, respectively.

1 Introduction

Cobalt-doped magnesium–aluminum spinel (Co^{2+}:$MgAl_2O_4$) is a well-known saturable absorber, which is used for generating passively Q-switched laser pulse in the eye-safe range of 1.5 μm [1, 2]. The Co^{2+}:$MgAl_2O_4$ crystal is a cubic crystal, and the anisotropy of nonlinear absorption in the Co^{2+}:$MgAl_2O_4$ crystal has been reported by Volk et al. [3]. However, the orientation of the transition dipoles within the $MgAl_2O_4$ crystal is still unknown. If the Co^{2+}:$MgAl_2O_4$ crystal is properly cut and then oriented in the laser cavity to consider intracavity field polarization, efficient passive Q-switch performance can be obtained.

The influence of the dipole orientations on nonlinear absorption has been studied in the cubic crystals such as Cr^{4+}:YAG [4–7], V^{3+}:YAG [8, 9], and F- 2:LiF [10]. The study of the absorption saturation of Cr^{4+} and V^{3+} ions in $Y_3Al_5O_{12}$ crystals showed that three groups of linear dipoles were oriented along three crystallographic axes, along the three fourfold axes of the unit cell [4–9]. When the incident polarized light propagates along with one of the crystallographic axes, the transmission shows four peaks and troughs during rotation of the crystal plate through 360°. When the incident polarized light propagates along with the [110] crystallographic axis, two maximum peaks and two submaximum peaks are observed. A more complicated situation is observed in F- 2:LiF crystal [10]. Studies have shown that six groups of linear dipoles were oriented along the six facet diagonals of the unit cell, along the six twofold axes of the unit cell. When the incident polarized light propagates along with [100] crystallographic axis, eight peaks and troughs are observed. All the above studies show that the anisotropy of nonlinear absorption of a cubic crystal is mainly determined by the orientation distribution of the transition dipoles. Different orientations of the transition dipoles in a cubic crystal will make the nonlinear absorption anisotropy different.

In 2007, Y. V. Volk et al. reported the anisotropy of transmission of Co^{2+}:$MgAl_2O_4$ single crystal at 1.54 μm [3]. The dependence of the transmission of a [100]-cut Co^{2+}:$MgAl_2O_4$ crystal on the polarization direction was investigated. Four peaks and troughs were observed during the rotation of the crystal plate through 360°. Maximal transmission was observed when the light polarization vector was parallel to the [100] or [010] crystallographic axis. However, the Co^{2+}:$MgAl_2O_4$ crystals cut in other directions (such as [110]), either the orientation of the transition dipoles, were not investigated.

✉ Qiang Li
ncltlq@bjut.edu.cn

1 Institute of Laser Engineering, Faculty of Materials and Manufacturing, Beijing University of Technology, Beijing 100124, China

2 Key Laboratory of Trans-Scale Laser Manufacturing Technology, Ministry of Education, Beijing 100124, China

3 Beijing Engineering Research Center of Laser Technology, Beijing 100124, China

4 Beijing Higher Institution Engineering Research Center of Advanced Laser Manufacturing, Beijing 100124, China

Until now, there are no further studies on the anisotropy of the nonlinear absorption in Co^{2+}:$MgAl_2O_4$ crystals have been reported.

In this paper, saturation absorption experiments were conducted on [100]- and [110]-cut Co^{2+}:$MgAl_2O_4$ crystals at 1.54 μm. A phenomenological model was established to analyze the experimental measurement results, in which the transition dipoles in the Co^{2+}:$MgAl_2O_4$ crystal are oriented along the four body diagonals ([111], [1 11], [1 1 1] and [11 1] axis) of the unit cell. The absorption cross-sections of the ground state and excited state of the Co^{2+}:$MgAl_2O_4$ crystal were also calculated using the model to support experimental data.

2 The samples investigated and experimental method

Two spinel Co^{2+}:$MgAl_2O_4$ crystals were investigated in the experiment, which were cut in two different directions, as shown in Fig. 1. The [100]-cut Co^{2+}:$MgAl_2O_4$ crystal had a thickness of 1.90 mm with an initial transmission of 0.86. The [110]-cut Co^{2+}:$MgAl_2O_4$ crystal had a thickness of 1.41 mm with an initial transmission of 0.90. The crystals were mounted on the rotation mounts, allowing their rotation around the axis of laser propagation direction (Fig. 1, ***r*** direction). The angle between the [001] crystallographic axis and the electric vector of the incident light was introduced as α. The initial position of the crystals was set so that the [001] crystallographic axis was parallel to the electric vector of the pump light. The transmissions of the saturable absorbers were calculated as a ratio of the transmitted energy to the input energy.

The experimental setup is shown in Fig. 2. The samples were excited by pulses from the passively Q-switched 1.54 μm laser. The pulse energy was 200 μJ, pulse duration was 4.5 ns with a 1 Hz repetition rate. A linearly polarized beam can be obtained after the laser beam passes through the polarization beam splitter (PBS). The incident energy fluence can be changed by rotating the half-wave plate (HWP). To overcome the influence of the laser energy fluctuation on the measurement, we used the two-channel detection method. The pump beam was focused on the Co^{2+}:$MgAl_2O_4$ crystals by the use of a combination of two focus lenses with focal lengths of 200 mm and 100 mm. The focused spot diameter of the pump beam was about 56 μm. And the maximum pump energy fluence was about 8 J/cm^2, which can saturate the experimental Co^{2+}:$MgAl_2O_4$ crystals.

3 Results and discussion

In the experiment, we maximized the amplitude of the anisotropic transmission modulation by adjusting the energy fluence. When the energy fluence was too low or too high, the transmission of the two Co^{2+}:$MgAl_2O_4$ crystals almost remained the same through a full 360° rotation. Obvious amplitude of the anisotropic transmission modulation was obtained as the energy fluence $E = 1.5$ J/cm^2 for [100]-cut crystal and $E = 2.5$ J/cm^2 for [110]-cut crystal. Figure 3 shows the measurement results of the two crystals. In Fig. 3a, for the [100]-cut Co^{2+}:$MgAl_2O_4$ crystal, the transmission changed periodically with the angle α (red hollow dots). There were four cycles through a full 360° rotation of the angle range, and each cycle had a peak and trough transmission. When α was 45°, 225° and 135°, 315°, the electric vector was parallel or perpendicular to the [110] crystallographic axis. In this case, the transmission peaks were observed. The transmission trough appeared when the electric vector was parallel to the [100] or [010] crystallographic axis ($\alpha = 0°$, 180° and 90°, 270°, respectively). The above measurement results are similar to those of the

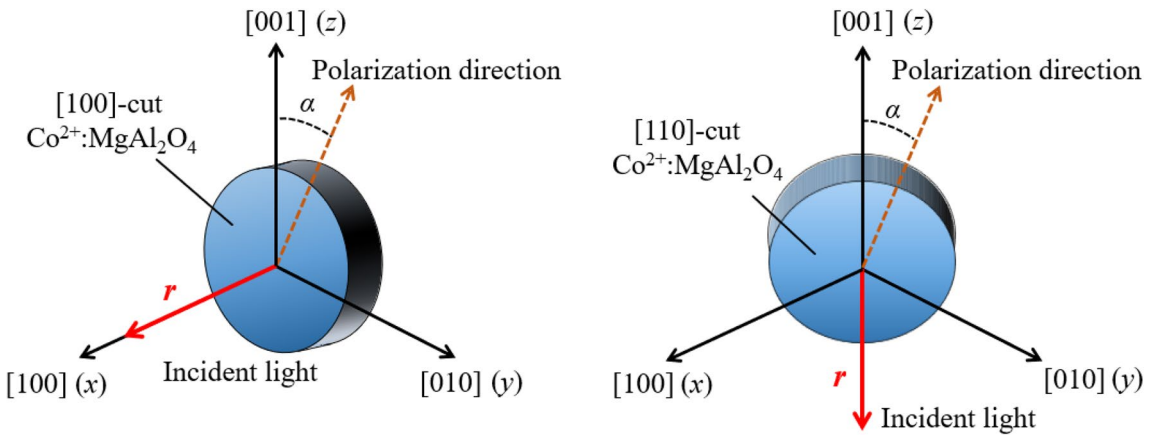

Fig. 1 Representation of orientation of the Co^{2+}:$MgAl_2O_4$ crystal plates with regard to the crystallographic axes. **a** [100]-cut; **b** [110]-cut

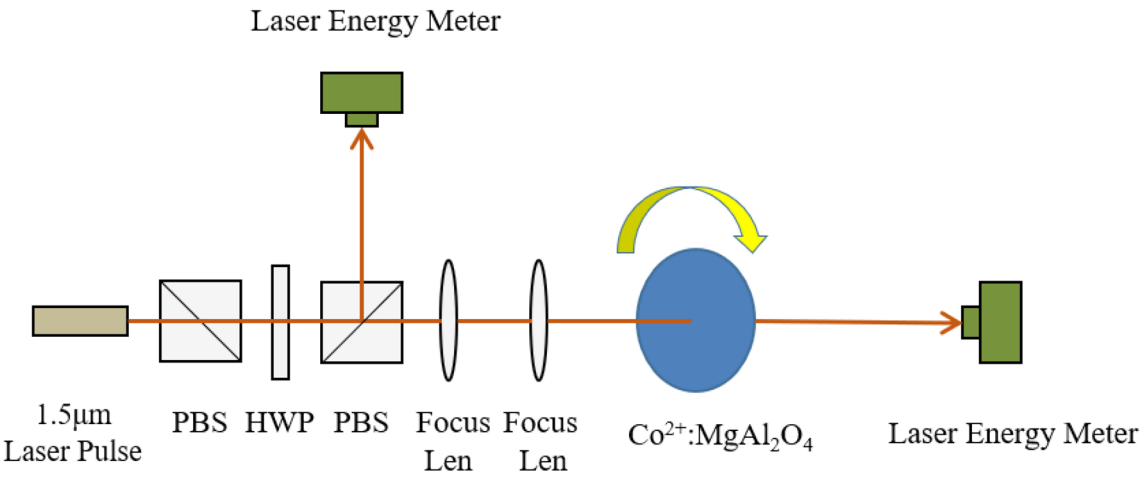

Fig. 2 Experimental setup for investigation of transmission

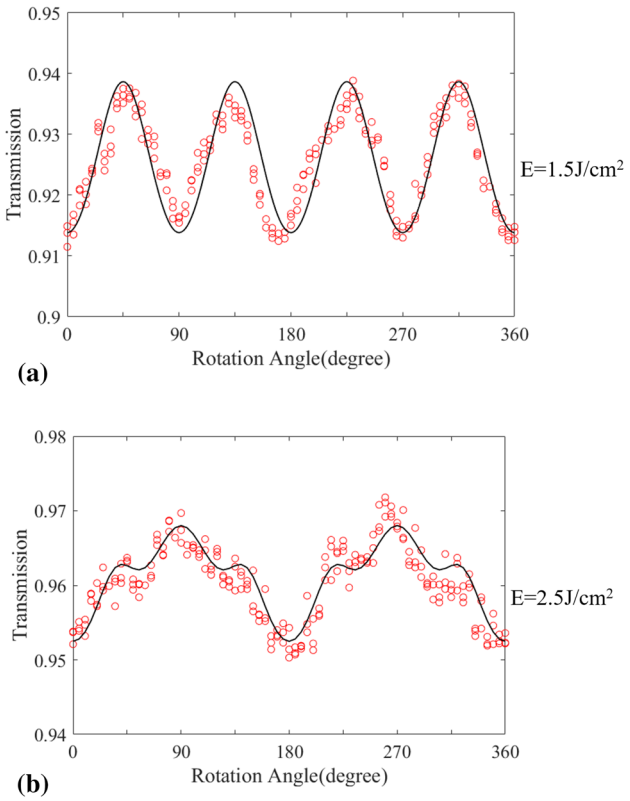

Fig. 3 The nonlinear transmission of the two crystals on the angle α between the crystallographic axis and the polarization direction. **a** [100]-cut. **b** [110]-cut. Red hollow dots are the experimental values, solid curves are the calculation by use of Eq. (6)

[100]-cut Cr^{4+}:YAG crystal in Ref. [11] and the [100]-cut Co^{2+}:$MgAl_2O_4$ crystal in Ref. [3], but the angles α corresponding to the transmission peaks and troughs are reversed. In Fig. 3(b), for the [110]-cut Co^{2+}:$MgAl_2O_4$ crystal, the transmission also varied periodically with the angle α (red hollow dots). There were two cycles in a full 360° rotation, and each cycle had a maximum value, two sub-maximum values, one minimum value, and two sub-minimum values. When α was 90° and 270°, the maximal transmission was observed. The minimal transmission appeared when α was 0° and 180°. In the case that α was 35°, 145°, 215° and 325°, the transmission reached the sub-maximum value. The sub-minimum transmission was observed when α was 55°, 125°, 235° and 305°. Similar to the [110]-cut Cr^{4+}:YAG, there is only one transmission peak in a full 360° rotation, but the angle α corresponding to the transmission peak is different. Studies have shown that stable and polarized laser pulses can be obtained using a [110]-cut Cr^{4+}:YAG crystal as the saturable absorber [11, 12], and maybe so can the [110]-cut Co^{2+}:$MgAl_2O_4$ crystal.

The anisotropy of nonlinear absorption of Co^{2+}:$MgAl_2O_4$ is determined by its crystal structure [5]. Considering the symmetry of a cubic crystal [13], the electric dipole can be oriented along one of 12/*m* possible *m*-fold axes ($m=4$, 3, 2). The unit cell of the spinel $MgAl_2O_4$ crystal belongs to the space group $Fd3m$ [14]. The O^{2-} anion sublattice is arranged in a pseudo-cubic close-packed (ccp) spatial arrangement, forming 96 interstices, but only the 24 interstices are occupied by cations. The divalent Mg^{2+} ions occupy one-eighth of the 64 tetrahedral interstices. Half of the 32 octahedral interstices are occupied by the trivalent Al^{3+} ion. The doping Co^{2+} ions substitute for tetrahedral coordinated Mg^{2+} ions [15], which are located at 8a Wyckoff Position (WP) with site symmetry $\bar{4}$ 3 *m* [14]. In other words, WP 8a contains three fourfold inversion symmetry axes (S_4-axes) parallel to the three crystallographic axes and four three-fold symmetry axes (C_3-axes) parallel to the [111]-, [1 $\bar{1}$ 1]-, [1 1 1]- and [11 1]-axis, as shown in Fig. 4a. According to Ref. [14], the distances between WP 8a and the four nearest-neighbor O^{2-} ions (0.21606*a*) are much smaller than

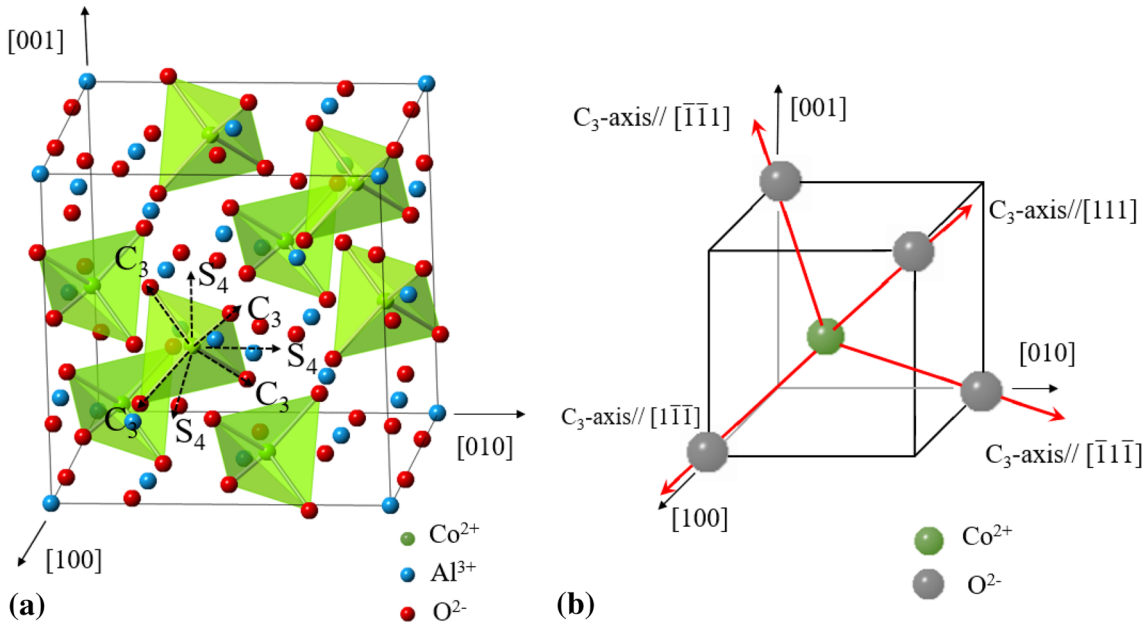

Fig. 4 **a** Unit cell of Co^{2+}:$MgAl_2O_4$ crystal. **b** 4 C_3-axes of tetrahedral coordinated Mg^{2+} ions, which parallel to the [111]-, [1 1̄1]-, [1 1 1̄]- and [11 1]-axis

the distances between WP 8a and other sites (0.41478*a* and 0.433013*a*). Therefore, we suppose that the Co^{2+} ions are more likely to form electric dipoles with the four nearest-neighbor O^{2-} ions, that is, the transition electric dipoles in the Co^{2+}:$MgAl_2O_4$ crystal are oriented along the four body diagonals of the unit cell, as shown in Fig. 4b. In addition, we assume that the transition dipole moments in each direction are equal.

To verify the proposed assumption, we established a phenomenological model of the Co^{2+}:$MgAl_2O_4$ crystal [3], in which the transition dipoles were oriented along the four body diagonals of the unit cell. The nonlinear transmission curves of [100]- and [110]-cut Co^{2+}:$MgAl_2O_4$ crystals on the angle α were calculated by this model, and the calculated results were compared with the experimental measurement results. If the calculated results are consistent with the measurement results, the assumption can be verified.

Firstly, according to the characteristics of the Co^{2+}:$MgAl_2O_4$ crystal, the phenomenological model was established as follows. The Co^{2+}:$MgAl_2O_4$ crystal is a slow-relaxing saturable absorber. In comparison with the lifetime (350 ns) of the metastable excited state, the relaxation time is rather short. So only the density in the ground state and the metastable excited state was considered. The excited-state absorption of the Co^{2+}:$MgAl_2O_4$ crystal was also considered. The coordinate system (x, y, z) chosen for calculation below are shown in Fig. 1. The incident light intensity I, passing through the Co^{2+}:$MgAl_2O_4$ crystal with the thickness of l, satisfies the following rate equation [5, 16]

$$\frac{1}{v}\frac{\partial I}{\partial t}+\frac{\partial I}{\partial r}=-\sum_{i=1}^{4}\left[\sigma_{\mathrm{gsa}}f_i(\alpha)N_{0i}+\sigma_{\mathrm{esa}}f_i(\alpha)N_{1i}\right]I \tag{1}$$

$$\frac{\partial N_{0i}}{\partial t}=-\frac{N_{0i}I\sigma_{\mathrm{gsa}}f_i(\alpha)}{h\nu}+\frac{N_{1i}}{\tau_1} \tag{2}$$

$$N_{0i}+N_{1i}=N_i, i=1,2,3,4 \tag{3}$$

where, ν is the speed of light, i is the number of types of center orientations, σ_{gsa} and σ_{esa} are ground- and excited-state cross-sections along the transition dipoles, $N_{0i}(r,t)$ and $N_{1i}(r,t)$ are the population with i-type orientation in the ground and metastable excited state, $N_i(r,t)$ is the total concentration of centers with i-type orientation, $f_i(\alpha)=\left(\boldsymbol{a_i}\cdot\boldsymbol{e}\right)^2$ is a factor representing the impact of the incident beam on the i-type transition dipoles, $\boldsymbol{a_i}$ and $\boldsymbol{e}$ are the unit vectors corresponding to the i-type electric dipoles and the electric field, respectively, τ_1 is the lifetime of the metastable excited state, $h\nu$ is the energy of a light quantum.

By solving the Eqs. (1), (2) and (3) analytically, we can obtain the expression for transmission of the saturable absorber versus input energy fluence U:

$$\frac{dU}{dr} = \sum_{i=1}^{4} N_i \left\{ \frac{h\nu\left(\sigma_{\mathrm{gsa}} - \sigma_{\mathrm{esa}}\right)}{\sigma_{\mathrm{gsa}}} \left[\exp\left(-\frac{U(r)\sigma_{\mathrm{gsa}} f_i(\alpha)}{h\nu}\right) - 1\right] - U(r)\sigma_{\mathrm{esa}} f_i(\alpha) \right\} \tag{4}$$

As mentioned above, we assume that the dipoles in the Co^{2+}:$MgAl_2O_4$ crystal are oriented along the four body diagonals of the unit cell. So unit vectors of the i-type electric dipoles are obtained as $\boldsymbol{a}_1 = \sqrt{3}(1,1,1)/3$, $\boldsymbol{a}_2 = \sqrt{3}(1,-1,-1)/3$, $\boldsymbol{a}_3 = \sqrt{3}(-1,1,-1)/3$, $\boldsymbol{a}_4 = \sqrt{3}(-1,-1,1)/3$. The small signal transmission T_0 can be obtained from Eq. (4):

$$T_0 = \exp\left(-4l\sigma_{\mathrm{gsa}} N_i/3\right) \tag{5}$$

Substitute Eq. (5) into Eq. (4), we can obtain

$$\frac{dU}{dr} = \sum_{i=1}^{4} \frac{-3\ln T_0}{4l\sigma_{\mathrm{gsa}}} \left\{ h\nu\left(1 - \frac{\sigma_{\mathrm{esa}}}{\sigma_{\mathrm{gsa}}}\right)\left[\exp\left(-\frac{U\sigma_{\mathrm{gsa}} f_i(\alpha)}{h\nu}\right) - 1\right] - U\sigma_{\mathrm{esa}} f_i(\alpha) \right\} \tag{6}$$

As shown in Fig. 1, the unit vectors of the electric field were obtained as $\boldsymbol{e} = (0, \sin\alpha, \cos\alpha)$ for [100]-cut crystal, and $\boldsymbol{e} = (-\cos 45° \sin\alpha, \sin 45° \sin\alpha, \cos\alpha)$ for [110]-cut crystal. Substituting those parameters into Eq. (6), the theoretical transmission curves as a function of the rotation angle α for [100]- and [110]-cut Co^{2+}:$MgAl_2O_4$ crystals can be obtained.

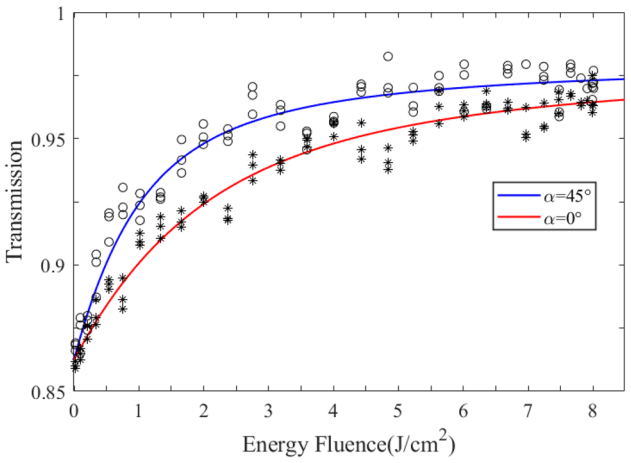

Fig. 5 The transmission curves on input energy fluences for [100]-cut Co^{2+}:$MgAl_2O_4$ crystal. Black hollow dots and asterisks are the experimental values, blue and red solid lines are the results of the fitting of the experimental data at the angles α were 0° and 45°, respectively, with the aid of Eqs. (7)–(8)

$$\frac{dU}{dr} = \frac{-3\ln T_0}{l\sigma_{\mathrm{gsa}}} \left\{ h\nu\left(1 - \frac{\sigma_{\mathrm{esa}}}{\sigma_{\mathrm{gsa}}}\right)\left[\exp\left(-\frac{U\sigma_{\mathrm{gsa}}}{3h\nu}\right) - 1\right] - \frac{U\sigma_{\mathrm{esa}}}{3} \right\}, \alpha = 0° \tag{7}$$

$$\frac{dU}{dr} = \frac{-3\ln T_0}{4l\sigma_{\mathrm{gsa}}} \left\{ h\nu\left(1 - \frac{\sigma_{\mathrm{esa}}}{\sigma_{\mathrm{gsa}}}\right)\left[\exp\left(-\frac{2U\sigma_{\mathrm{gsa}}}{3h\nu}\right) - 2\right] - \frac{4U\sigma_{\mathrm{esa}}}{3} \right\}, \alpha = 45° \tag{8}$$

Secondly, to solve the Eq. (6), we conducted the following saturation experiments to calculate the ground- and excited-state absorption cross-sections at 1.54 μm. The experimental setup is shown in Fig. 2. The input energy fluence can be changed by rotating the half-wave plate, and the pump energy fluence can be varied from 0 to 8 J/cm^2. The [100]-cut Co^{2+}:$MgAl_2O_4$ crystal with the initial transmission $T_0 = 0.86$ was used. Figure 5 shows the transmission of the sample in relation to the input fluence for light polarization corresponding to the maximal transmission ($\alpha = 45°$, black hollow dots) and to the minimal transmission ($\alpha = 0°$, black asterisks). The dependences at the two angles started from the equal small-signal transmission. When α was 45°, the light polarization was parallel to the [110] crystallographic axis, and the sample was easier to reach absorption saturation. Then we fit the theoretical dependences to the experimental data in Fig. 5. We substituted the angles $\alpha = 0°$ and $\alpha = 45°$ into Eq. (6), and we can obtain

The Eqs. (7)–(8) were used to calculate theoretical dependences of transmission of [100]-cut Co^{2+}:$MgAl_2O_4$ crystal on the input fluence at the two angles, respectively. The best fits (Fig. 5, blue and red solid lines) to the experimental data (Fig. 5, black hollow dots and asterisks) were obtained with the values of the $\sigma_{\mathrm{gsa}} = (3.6 \pm 0.3) \times 10^{-19}$ cm^2 and $\sigma_{\mathrm{esa}} = (4.5 \pm 0.4) \times 10^{-20}$ cm^2. The obtained absorption cross-sections are in good agreement with Refs.

[2, 3, 17]. The ground state absorption cross-section is smaller in comparison with that in Ref. [3], and the difference may be due to the different assumptions about the orientation of the transition dipoles in the Co^{2+}:$MgAl_2O_4$ crystal. In the model of this paper, when the pump light propagates along with one of the crystallographic axes, the electric dipoles oriented along the four body diagonals will all interact with the pump light. However, in Ref. [3], the transition dipoles are assumed to be along the three crystallographic axes. When the pump light propagates along with one of the crystallographic axes, only one group of the linear dipoles, which is oriented along this crystallographic axis, will interact with the pump light. Therefore, the measured absorption cross-section becomes larger.

Finally, substituting absorption cross-sections of the ground state and excited state obtained above into Eq. (6), the theoretical dependences of nonlinear transmission T on the rotation angle α were obtained. The fitting curves (black solid lines) are shown in Fig. 3, including [100]- and [110]-cut Co^{2+}:$MgAl_2O_4$ crystals. The calculated results are in good accordance with the measurement results, which verifies the assumption that the transition dipoles in the Co^{2+}:$MgAl_2O_4$ crystal are mainly oriented along the four body diagonals of the unit cell.

However, this paper simply considered the absorption cross-sections along the π direction. Due to the symmetry of the crystal structure, the absorption cross-sections along the σ direction also should be considered. We are presently using higher-precision measurement techniques, such as the Pump–probe technique, to conduct a more in-depth analysis of the absorption saturation of the Co^{2+}:$MgAl_2O_4$ crystal.

4 Conclusion

In this paper, the experiments and theoretical simulations have demonstrated that the transition dipoles in the Co^{2+}:$MgAl_2O_4$ crystal are mainly oriented along the four body diagonals ([111], [1 $\bar{1}$ 1], [1 1 $\bar{1}$] and [$\bar{1}$1 1] axis) of the unit cell. The absorption cross-sections of the ground state and excited state of the Co^{2+}:$MgAl_2O_4$ crystal are calculated to be $\sigma_{gsa} = (3.6 \pm 0.3) \times 10^{-19}$ cm^2 and $\sigma_{esa} = (4.5 \pm 0.4) \times 10^{-20}$ cm^2, respectively. The determination of the orientation of the electric dipoles and measurement of the ground- and excited-state absorption cross-sections in the Co^{2+}:$MgAl_2O_4$ crystal can provide great help in the application of passively Q-switched lasers at 1.5 μm. By choosing a crystal cut in a special direction, such as [110], there is only one maximum transmission peak on the plane perpendicular to the direction of incident light. And the laser is easy to oscillate in this direction. The polarization of the passively Q-switched laser is along this direction and the oscillation state becomes stable, which can further improve the output characteristics of passively Q-switched lasers such as extinction ratio and stability. We are presently conducting experiments to investigate the impact of Co^{2+}:$MgAl_2O_4$ crystal cut in special directions on the laser output performances.

Acknowledgements This work was supported by the Natural Science Foundation of Beijing Municipality (Grand No. 4202007 and KZ202110005010), the National Natural Science Foundation of China (Grand No. 62075003).

Data availability The datasets generated during the study are available from the corresponding author on reasonable request.

References

1. K.V. Yumashev, Appl. Opt. **38**, 6343 (1999)
2. K.N. Gorbachenya, V.E. Kisel, A.S. Yasukevich, V.V. Maltsev, N.L. Leonyuk, N.V. Kuleshov, Opt. Lett. **41**, 918 (2016)
3. Y.V. Volk, A.M. Malyarevich, K.V. Yumashev, V.N. Matrosov, T.A. Matrosova, M.I. Kupchenko, Appl. Phys. B **88**, 443 (2007)
4. H. Eilers, K.R. Hoffman, W.M. Dennis, S.M. Jacobsen, W.M. Yen, Appl. Phys. Lett. **61**, 2958 (1992)
5. A.G. Okhrimchuk, A.V. Shestakov, Phys. Rev. B **61**, 988 (2000)
6. M. Tsunekane, T. Taira, IEEE J. Quantum Electron. **52**, 1 (2016)
7. Y. Sato, T. Taira, Opt. Mater. Express **7**, 577 (2017)
8. N.N. Il'ichev, A.V. Kir'yanov, P.P. Pashinin, V.A. Sandulenko, A.V. Sandulenko, S.M. Shpuga, Quantum Electron. **25**, 1154 (1995)
9. V. Laguta, M. Buryi, A. Beitlerova, O. Laguta, K. Nejezchleb, M. Nikl, Opt. Mater. **91**, 228 (2019)
10. N.N. Il'ichev, A.V. Kir'yanov, A.A. Malyutin, P.P. Pashinin, S.M. Shpuga, Laser Phys. **3**, 182 (1993)
11. H. Sakai, A. Sone, H. Kan and T. Taira, in Advanced Solid-State Photonics, Technical Digest (Optical Society of America, 2006), paper MD2
12. R. Bhandari, T. Taira, Opt. Express **19**, 22510 (2011)
13. N.N. Il'ichev, A.V. Kir'yanov, P.P. Pashinin, S.M. Shpuga, J. Exp. Theor. Phys. **78**, 768 (1994)
14. K.E. Sickafus, J.M. Wills, J. Am. Ceram. Soc. **82**, 3279 (1999)
15. N.V. Kuleshov, K.P. Mikhailov, V.G. Scherbitsky, P.V. Prokoshin, K.V. Yumashev, J. Lumin. **55**, 265 (1993)
16. Y.K. Kuo, M.F. Huang, M. Birnbaum, IEEE J. Quantum Electron. **31**, 657 (1995)
17. V.G. Shcherbitsky, S. Girard, M. Fromager, R. Moncorge, N.V. Kuleshov, V.I. Levchenko, V.N. Yakimovich, B. Ferrand, Appl. Phys. B **74**, 367 (2002)